PCCP

Accepted Manuscript

ROYAL SOCIETY OF CHEMISTRY

www.rsc.org/pccp

PCCP

RSCPublishing

ARTICLE

A Combined ^{77}Se NMR and Molecular Dynamics Contribution to the Structural Understanding of the Chalcogenide Glasses

Cite this: DOI: 10.1039/xoxxooooox

Received ooth January 2012,
Accepted ooth January 2012

DOI: 10.1039/xoxxooooox

www.rsc.org/

Kateryna Sykina,[a] Bruno Bureau,[b] Laurent le Pollès, [b] Claire Roiland,[b] Michaël Deschamps, [c] Chris J. Pickard,[d] and Eric Furet [a,*]

Solid-state ^{77}Se NMR measurements, first-principles molecular dynamics and DFT calculations of NMR parameters were performed to gain insight into the structure of selenium-rich $Ge_xSe_{(1-x)}$ glasses. We measured fully-relaxed NMR spectra on natural abundance and 100% isotopically enriched $GeSe_4$ samples, which led us to reconsider the level of structural heterogeneity in this material. In this paper, we propose an alternative procedure to initialise molecular dynamics runs for the chalcogenide glasses. The ^{77}Se NMR spectra calculated on the basis of the structural models deduced from these simulations are consistent with the experimental spectrum.

Introduction

The chalcogenide glasses are known to exhibit a wide range of physical properties (high linear and nonlinear refractive indexes, large infrared transparency windows, reversible amorphous-to-crystal transition), some of which being unique to them such as various light-induced phenomena.[1] Due to the weak stoichiometric constraints on amorphous materials, these electrical, mechanical or optical properties may be easily tuned by composition modulation. These features have paved the way to a large spectrum of technological applications including non-volatile memories, optical data storage, infrared lenses and fibers, gratings, planar waveguides.[2] Recently, they have also been considered as viable materials to build thermoelectrical devices.[3] Despite their large domain of technological applications, chalcogenide glass structures are not so well-known because most of experimental data obtained from spectroscopic tools are not straightforward to interpret. Even for glasses in the prototypical binary Ge-Se system that have been intensively studied using various experimental characterization techniques,[4–7] the debate continues.

In recent years, solid-state ^{77}Se NMR investigations have been carried out in order to get a better understanding of the structure of $Ge_xSe_{(1-x)}$ glasses. In the specific case of the $GeSe_4$ composition which is known to be the best glass former of the Ge-Se system, and moreover to correspond to a structural threshold in the Thorpe's counting scheme,[8] significant progresses have been made by Bureau *et al*[7,9] and Sen *et al.*[10–12] Their results have allowed the unambiguous elimination of the homogeneous model called the *chain crossing model (CCM)* in which the glass structure is built up from evenly distributed $GeSe_{4/2}$ tetrahedra and Se chains whose lengths increase with chalcogen content. In the case of g-$GeSe_4$, this model predicts the existence of selenium dimers connecting the $GeSe_4$ tetrahedra, leading therefore to the following theoretical percentages for the Se environments : 0 (Se-**Se**-Se); 0 (Ge-**Se**-Ge) and 100% (Ge-**Se**-Se) and hence would lead to a single peak in the ^{77}Se NMR spectrum which is in contradiction with the observed double peak measured by Bureau *et al*[7,9] and Sen *et al.*[10–12]

Nowadays, two different models are discussed to describe the structure of selenium-rich $Ge_xSe_{(1-x)}$ glasses ($x<1/3$). In their investigation, Bureau *et al* concluded that the fraction of Ge-**Se**-Se might be neglected, leading to a *bimodal percolation model* (*BP*) in which a phase separation occurs at a local scale between g-Se and g-$GeSe_2$ domains.[7,9] In the $GeSe_2$ phase, $GeSe_{4/2}$ tetrahedra share selenium atoms through corners (CS) or edges (ES), leading to a significant amount of Ge-**Se**-Ge (CS&ES) units. Then, Sen *et al* refined this first ^{77}Se NMR input and concluded that up to ~25% of Ge-**Se**-Se environments could be identified based on the Magic Angle Spinning spectra (Table 1).[10,11] This led them to propose a *randomly connected model* (*RC*) in which Se chains of various lengths interconnect clusters of CS and/or ES germanium polyhedra.

On the theoretical investigations side, Kibalchenko *et al* have recently performed molecular dynamics calculations coupled to NMR simulations to get some clues on g-$GeSe_2$ and g-$GeSe_4$.[13] Due to the lack of resolution of the experimental $GeSe_2$ spectrum, not much could be said on the theoretical side. One of their main conclusions was that molecular dynamics simulations led to overly disordered samples, as they obtained

in the case of g-$GeSe_4$ 46% of Ge-**Se**-Se environments, that precluded them from reproducing the experimental spectrum. This led them to perform a deconvolution of the experimental spectrum of g-$GeSe_4$ measured by Sen's *et al*, on the basis of the computed isotropic chemical shifts for five different kinds of Se environments found in the simulated glass. Adding results obtained by Raman scattering, they suggested a distribution of the various selenium environments in g-$GeSe_4$ that was quite close to the values deduced by Sen *et al*.

In the context of a continuous effort by several groups to get a better understanding of the structure of chalcogenide glasses, we will describe here the results of new ^{77}Se NMR investigations performed on both natural abundance and 100% ^{77}Se enriched $GeSe_4$ samples. In parallel, molecular dynamic (MD) simulations have been carried out to generate *in silico* $GeSe_4$ structures following different strategies. Then, the ^{77}Se NMR parameters were computed for each selenium atom and the $GeSe_4$ NMR spectra have been reconstructed by simulating the NMR lineshape of each Se atom. Finally, the theoretical spectra were compared to the experimental signal in order to decide which MD strategy gives the better account of the $GeSe_4$ glassy network. We will show in the following sections that a good agreement can be achieved between the new experimental ^{77}Se spectra and those deduced from the theoretical structures obtained by means of an updated MD procedure that we used to build the starting configurations.

Experimental and Theoretical Methods

Raw materials with 99.999% elemental abundances were used for glass preparation. The mixture of the required amounts of Se and Ge were sealed in a silica tube under vacuum and then maintained at 850°C for 12 hours in a rocking furnace to ensure a good mixing and homogenization of the liquid. To maximize vapour condensation into the liquid phase, the temperature was reduced to 650°C for 1 hour. Then the ampoules were quenched in water and annealed near glass transition temperatures (T_g=165°C for $GeSe_4$) to reduce the mechanical stresses that occur upon cooling. The glassy nature was confirmed by X-ray diffraction and differential scanning calorimetry (DSC), and the final stoichiometry was checked by EDS. The same procedure has been used for the 100% ^{77}Se enriched $GeSe_4$ sample made from a smaller batch (about 200 mg) due to the cost of ^{77}Se-isotopically enriched selenium.

The Hahn echo spectra of the ^{77}Se-enriched $GeSe_4$ sample was recorded in a 7T Bruker NMR spectrometer (300 MHz for ^{1}H), in a 3.2 mm double resonance MAS probe at a MAS rate of 23 kHz. A 100 kHz RF field strength was used, and the recovery delay was set to 90 seconds (corresponding to more than than 1.5 times the longitudinal relaxation time T_1). The Hahn echo delay was set to 1 rotor period to avoid T_2-induced distortions of the NMR spectra. Using the same setup, a ^{77}Se Carr-Purcell-Meiboom-Gill[14] (CPMG) NMR spectrum was acquired on a natural abundance sample and 32 echoes acquired with 600 microseconds between each 180° refocusing pulse, and 64 scans were used with a recovery delay of 900 seconds. Furthermore, natural abundance ^{77}Se spectra were also recorded at the same static field using rotor synchronized Hahn echo pulse sequences. To increase the signal to noise ratio, we employed a 4 mm MAS probe at a spinning rate of 12 kHz with a 60 kHz RF field. As discussed in this paper, variable recyle delays up to 1200 seconds were employed. The ^{77}Se chemical shift was referenced to H_2SeO_3 saturated in water at 1288 ppm.

All Car-Parrinello molecular dynamics simulations have been performed with the CPMD-3.15.3 package,[15–17] using the Perdew-Burke-Ernzerhof exchange and correlation functionals,[18] on a cubic simulation cell of 18.3 Å^3 containing 215 atoms. The integration step for the simulations was chosen to be equal to 7 a.u. (0.17 fs), and the fictitious electronic mass was taken to be equal to 850 a.u. Norm conserving pseudopotentials of the Troullier-Martins type[19,20] were employed to describe the core electrons of the germanium and selenium atoms. The plane-wave basis sets were expanded up to a kinetic energy cut-off of 20 Ry and the calculations were carried out at the Γ point of the Brillouin zone. The temperature was controlled by means of Nose-Hoover chain thermostats.[21,22] The synthesis of the glasses *in silico* was done through the following process : the cells were equilibrated in the liquid state (T = 900 K) for up to 100 ps (see Figure S1) and were gradually quenched in plateaus of dozens of ps separated of 200 K. The statistical averages were then collected at T=300 K for at least 30 ps.

The ionic positions of the configurations used for the NMR parameters calculations have been optimized with the CPMD program, by means of the BFGS algorithm. The criteria for the total energy and the maximum gradient component were set to $1x10^{-7}$ a.u. and $5x10^{-6}$ a.u. respectively. Figure S2 shows that performing the same task with the CASTEP program gives essentially the same lineshape, the whole spectrum being only slightly shifted.

All ^{77}Se NMR parameters were computed using the *gauge including projector augmented wave* (GIPAW) formalism[23] as implemented in the CASTEP package,[24] version 5.5.2. The Perdew-Burke-Ernzerhof exchange and correlation functional,[18] on-the-fly generated ultrasoft pseudopotentials, and an expansion of the plane-wave basis sets up to an energy cutoff of 350 eV (25.7 Ry) was used. The Brillouin zone was sampled with a 2x2x2 k-points grid. The convergence of the NMR parameters was checked by performing calculations on a sample cell up to 600 eV. As shown in figure S3 (top), the spectrum is negligibly affected upon going from 350 eV to 600 eV. The mean and standard deviation values of the isotropic chemical shielding variations for the 350 eV calculation with respect to the 600 eV one are respectively equal to 1.3 and 0.8 ppm (Figure S3 - bottom). The GIPAW calculations give access to the absolute shielding tensor ($\boldsymbol{\sigma}$) and we perform a diagonalization of the symmetric part of $\boldsymbol{\sigma}$ to determine the three orthogonal principal components. Following the Haeberlen convention,[25] the three eigenvalues were ordered such that $|\sigma_{zz} - \sigma_{iso}| > |\sigma_{xx} - \sigma_{iso}| > |\sigma_{yy} - \sigma_{iso}|$ where $\sigma_{iso} = (\sigma_{xx} + \sigma_{yy} + \sigma_{zz})/3$. The reduced anisotropy (CSA) and asymmetry parameters (η) were computed as CSA = $\sigma_{zz} - \sigma_{iso}$ and $\eta = (\sigma_{yy}$

$-\sigma_{xx}$)/CSA respectively. The isotropic chemical shift is defined as $\partial_{iso} = \sigma_{ref} - \sigma_{iso}$, where σ_{ref} is the isotropic chemical shielding of the reference compound. Calculations on the α–selenium crystalline phase gave a σ_{ref} value equal to 1483 ppm that compares favourably with the 1494 ppm value determined by Kibalchenko *et al.*[26]

The spectra have been simulated with the Simpson program[27] which closely matches the NMR experiment as this software allows the emulation of the experimental acquisition process and explicitly takes into account the reduced anisotropy and asymmetry parameters in the simulations.

All the NMR parameters calculations in the present study have been performed within a non-relativistic framework, as it has already been shown by several authors, that the non-relativistic GIPAW method leads to accurate ^{77}Se isotropic chemical shifts.[13,26,28]

Results and discussion

Magic-Angle Spinning (MAS) solid-state NMR measurements have been performed for the first time on a 100% ^{77}Se isotopically enriched sample in order to improve the sensitivity and consequently the signal quality with respect to previous investigations. It should be recalled that the ^{77}Se (I=1/2) natural abundance is equal to 7.6% and that this isotope is moreover a relatively low-γ nucleus (5.125×10^{-7} rad.T^{-1}.s^{-1}). Figure 1 contains two ^{77}Se Hahn echo spectra acquired on an isotopically enriched sample using two different recovery delays (D1 = 90 and 720 s). We used a saturation-recovery experiment to measure the T_1 of ^{77}Se-enriched $GeSe_4$. Both the right and left hand sides of the spectrum relax with the same T_1 of around 75 seconds, and therefore we chose to record the ^{77}Se NMR spectrum with a recovery delay of 90 s to maximize the S/N ratio in a given experimental time without risking any line shape distortion. This choice is confirmed by the similarity between the two isotopically enriched spectra. Surprisingly, the T_1 for the left and right component are identical and shorter than in the natural-abundance samples (see below), most probably due to dipole-dipole cross-relaxation between the ^{77}Se spins in connection with the high density of NMR-active nuclei in that case.

With respect to previously published measurements[7,9–12] the corresponding spectra possess the same typical double-resonance lineshape, but interestingly, the peak associated to the Se chains (800 ppm) presents a lower relative intensity with respect to the signal at 400 ppm. Given that in the enriched sample, the magnetization transfer is greatly improved by spin diffusion due to the high concentration of NMR-active isotope, much higher recovery delays would be required with non-enriched samples. However, until then, the recovery delays used were at best equal or even lower to 60 s.[7,9–11] In order to check this assumption, a series of spectra was recorded on the natural abundance sample starting with a recovery delay of 60 s (2000 scans) and up to 1200 s (300 scans).

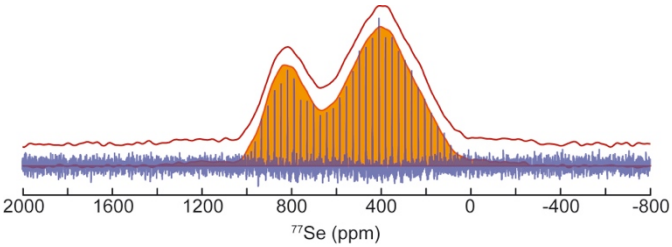

Fig. 1 Experimental ^{77}Se NMR spectra (B_o=7T) obtained on $GeSe_4$ glasses. (in blue - spikelets) CPMG NMR spectrum acquired on natural abundance sample with a recovery delay (D1) of 900 s (64 scans). (in orange, filled) Hahn echo spectrum measured on ^{77}Se-enriched sample with a D1 value of 90 s (512 scans). (in red on top) Hahn echo spectrum recorded on enriched $GeSe_4$, with a recovery delay of 720 seconds (128 scans). Very small sidebands are observed on the left and right hand side of the spectrum accounting for less than a few per cent of the centerbands. See the experimental method section for additionnal technical details.

Figure 2 shows that, as in previous studies, the peak corresponding to the Se-**Se**-Se chains dominates for D1 values lower than 300 s, *i.e.* five times the standard value used up to now. For recovery delays higher or equal to 600 s, the signal of the natural abundance sample can be considered to be fully-relaxed and the contributions stemming from selenium atoms bonded to germanium dominate in a fashion consistent with the measurements on the enriched sample.

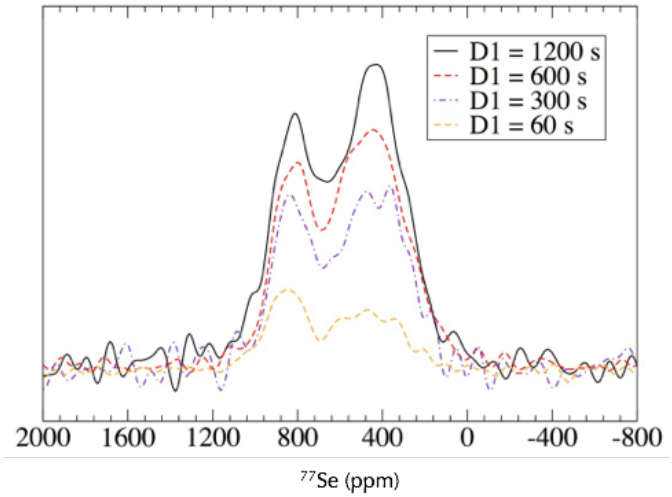

Fig. 2 Experimental ^{77}Se Hahn echo NMR spectra (B_o=7T) obtained for a natural abundance $GeSe_4$ glass sample (bottom) with recovery delay values between 60 s and 1200 s.

This work devoted to the impact of D1 parameter on the spectrum lineshape of the natural abundance sample, also offers the opportunity to have access to an estimate of the relaxation times (T_1) for the ^{77}Se in the Se-**Se**-Se and Ge-**Se**-X (X = Se, Ge) environments. We calculated for the selenium phase a T_1 value equal to 100-150s while from the peak associated to selenium atoms in the coordination sphere of germanium, the value is around 200-250s. This difference is consistent with the larger flexibility and consequently the greater mobility (a source of relaxation) of the Se chains with respect to the case of selenium atoms involved in corner- and/or edge-sharing germanium tetrahedra. Taken as a whole our results show that

the experiments performed with or without isotopically enriched samples lead to similar results, provided that appropriate recovery delays are used. More interestingly these experiments lead to a ^{77}Se NMR lineshape for $GeSe_4$ glasses significantly different from the signal presented in the literature. Our results show that ^{77}Se spin-lattice relaxation times in $GeSe_4$ are much longer than previously assumed. This implies that, for future works, such long recovery delays have to be used to access to quantitative informations from spectra collected on natural abundance samples.

Finally, it should be noted that a ^{77}Se CPMG NMR was acquired on a natural abundance $GeSe_4$ sample, as seen in figure 1. The spectrum obtained for a D1 value of 900 s perfectly match the one of the ^{77}Se-enriched sample (D1 = 90 s), giving therefore additional credit to the fact that we obtained fully relaxed spectra.

Considering our new spectrum, we focused on the second stumbling block corresponding to the discrepancy between theoretical and experimental ^{77}Se NMR spectra obtained on the basis of *in silico* generated glass, as pointed out by Kibalchenko *et al*[13] In a first stage, ^{77}Se NMR parameters have been computed on optimized configurations taken from earlier first-principles molecular dynamics calculations carried out on a cubic supercell containing 215 randomly distributed atoms (***H***).[29] These simulations performed using the PBE functional led to a lower fraction of Ge-**Se**-Se environments with respect to the Perdew-Wang results (Table 1). Moreover they offered notably the opportunity to investigate for possible size effects on the spectrum (96 *vs* 172 Se atoms).

Table 1 Distribution of the various Se environments (%) in the experimental models and molecular dynamics simulations.

	Exp. BP [9]	***Exp. RC*** [11]	***PW*** [13]	***PBE(H)*** [29]
Se-**Se**-Se	50±5	36±5	29	29
Ge-**Se**-Ge(CS+ES)	50±5	-	23	29
Ge-**Se**-Ge(CS)	-	38±5	16	19
Ge-**Se**-Ge(ES)	-	-	7	10
Ge-**Se**-Se	~0	26±5[a]	46	38
Se$_*$[b]	-	-	1	4

[a]Ge-Se-Ge(ES) sites counted with the Ge-**Se**-Se due to their similar ∂_{iso} values. [b]denotes all Se atoms deviating from the 8-N rule.

Figure 3 shows, in that case, an example of a ^{77}Se NMR spectrum obtained on the basis of the 172 individual Se signals that were simulated using the Simpson program.[27] Unfortunately, the lineshape lacks the typical double-peak feature found in all experimental spectra. However in agreement with experiments,[7,9] we note on the plus side that the average ∂_{iso} value for the selenium atoms in the chains is almost equal to 800 ppm, while it is close to ~450 ppm for those bound to germanium atoms. Additionally the width of the theoretical signal is rather accurately reproduced, being only slightly overestimated with respect to the experimental one. It is immediately seen, as found by Kibalchenko *et al,*[13] that the lineshape is almost entirely determined by the large fraction of Ge-**Se**-Se units (Table 1), resonating around 500 ppm, *i.e.* between the corner-sharing Ge-**Se**-Ge units and the selenium phase. Therefore the somewhat lower percentage of Ge-**Se**-Se units obtained in the PBE case is not sufficient to resolve the discrepancy noted between theory and experiment.

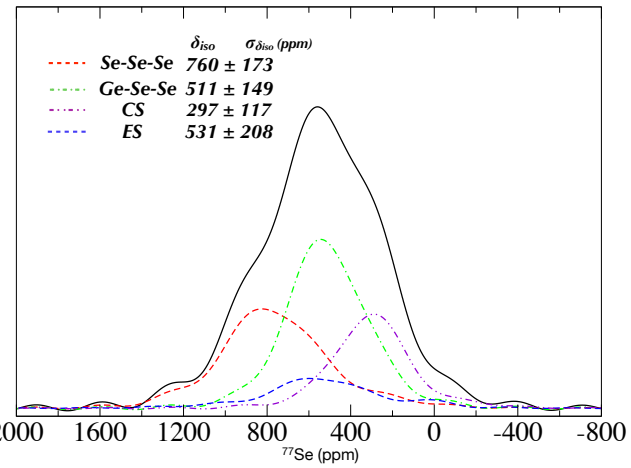

Fig. 3 ^{77}Se NMR (MAS 23 kHz) spectra simulated for an optimized configuration of the ***H*** glass model at 300 K. Contributions of different environments are given, together with the mean ∂_{iso} and standard deviations values.

From our point of view, this excess of Ge-**Se**-Se environments is the consequence of two simultaneous factors: i) the building process of the starting configurations in the so-called standard procedure, relies on a random distribution of germanium atoms in the cell, that are consequently too finely dispersed among the selenium matrix. ii) the independently formed $GeSe_4$ building blocks do not tend to spontaneously aggregate in clusters of edge and/or corned-sharing tetrahedra, due to the lack of a driving force that would therefore reduce the fraction of Ge-**Se**-Se units. As a consequence, the final structure of the simulated glass appears rather homogeneous, with short chains connecting small groups of GeX_4 tetrahedra (X = Se, Ge), and this excess of homogeneity does not allow to account for the experimental NMR lineshape.

Thus, while it may seem natural to start from an ideally homogeneous melt, *i.e.* at the atomic-scale, due to the fact that it allows to bypass the computationally costly mixing phase of the standard approach, this assumption may not be correct in the end. Experimentally, fine-grained powders of the raw materials are put together and undergo a homogeneisation process. Given the large difference in melting temperatures of Ge (T_f = 1211 K) and Se (T_f = 494 K), solid-liquid reactions that should promote the formation and linking of $GeSe_4$ tetrahedra at the interface of micron-sized germanium grains cannot therefore be discarded.

In an attempt to validate this hypothesis, several heterogeneous starting configurations have been built up. Two different shapes for the germanium phase have been considered. One in which it occupies an almost spherical volume (***G***) and a slab-like structure (***S***) that should have a higher specific surface area (Figure 4). Thereafter, $\boldsymbol{G}_a$ and $\boldsymbol{G}_b$, correspond to two independent starting configurations of the ***G*** model having different initial random ionic positions (see SI).

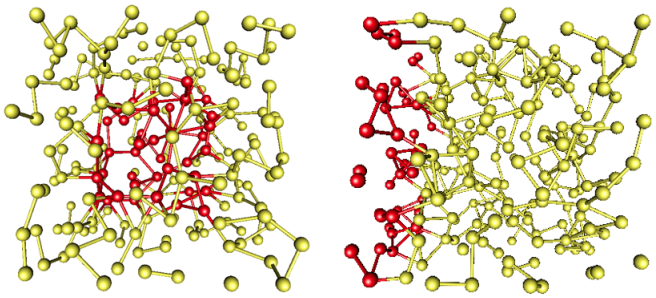

Fig. 4 Two examples of heterogeneous structures used as starting-points for the molecular dynamic simulations in the case of our new approach. Left : ***G*** model; Right : ***S*** model. The selenium atoms are shown in yellow, and the germanium atoms in red.

Concerning specifically this work on heterogeneous starting-points molecular dynamics, it must be stressed that having to explicitly simulate a mixing phase adds an additional question concerning the appropriate duration for the corresponding plateau. As with the so-called standard procedure, we have monitored the conserved energy until it oscillates around a mean value over several ps. However this is not sufficient with the heterogeneous approach. Given that our mixing stage is associated to the disappearance of the germanium block, the number of Ge-Ge bonds has also been monitored until it stabilizes (Figure S1 - Supporting Information).

The comparison of the radial distribution functions (RDF - $g_{X\text{-}Y}(r)$ – Figure S4) for the ***G***, ***S*** and ***H*** models at 300K shows that both approaches lead to very similar $g_{Ge\text{-}Se}$ and $g_{Se\text{-}Se}$ functions for distances below 4 Å. Concerning the Ge-Ge partial pair correlation functions, we observe in all cases, three peaks for r < 4 Å that are considered as the fingerprint of Ge-Se glasses.[30] Therefore the mean short-to-medium range order appears to be very similar between the various kinds of starting-points. We note however that heterogeneous cells may possess a somewhat higher first maximum that is associated to homopolar bonds. Table 2 that gathers statistical data for our models shows indeed that the fraction of Ge atoms involved in homopolar bonds is equal to 5% for an ***H*** glass, and is in the 5-12% range, when considering ***G*** or ***S*** structures. It is worth recalling that these ambient temperature values are obtained from heterogeneous configurations in which the Ge-Ge bond percentage is stabilized in the liquid state and oscillates between 5-15% (Figure S1).

The possible slightly higher fraction of Ge-Ge bonds at 300K should not be considered as an artifact resulting from an incomplete germanium phase melt, as the probability of having some homopolar bonds that stay trapped during the formation of the network of interconnected tetrahedra is higher with heterogeneous starting configurations. Consequently, the existence of a single $X_3Ge\text{-}GeX_3$ entity in the ***H*** case, corresponding to 2/43 (4.6% of the germanium atoms) gives some clues concerning a plausible lower bound that can probably only be achieved within an artificially homogeneous melting process. Indeed, the Ge-Ge graph of an ***H*** model at high temperature shows that a sole homopolar bond is cyclically detected in the simulation cell (Figure S1). As for the germaniun coordination modes, at first sight the ***H*** glass distribution appears narrower with respect to the ***G*** and ***S*** models. More than 94% of $GeSe_4$ units are indeed obtained in the former case. Nevertheless, the general tendency is common for all types of structures, as indeed at least 93% of Ge atoms are fourfolded, and the somewhat larger number of *e.g.* Ge-(Se_3Ge) tetrahedra in the ***G*** and ***S*** glasses being consistent with the slightly higher fraction of Ge-Ge bonds. It should be noted that this value is just above the 88% for the $GeSe_4$ tetrahedra found in the PW simulations.[29,30]

Table 2. Coordination modes of germanium atoms and homopolar bond fractions (%) in the various glass models. Values below 1% are not given. G_a and G_b correspond to two independent starting configurations of the ***G*** model.

	H	G_a	G_b	***S***
$Ge\text{-}Se_2$	-	1	1	-
$Ge\text{-}Se_3$	1	3	6	-
$Ge\text{-}Se_4$	94	82	88	89
$Ge\text{-}Se_3Ge$	5	9	5	9
$Ge\text{-}Se_2Ge_2$	-	2	-	-
$Ge\text{-}Se_5$	-	2	-	1
$Ge\text{-}Se_4Ge$	-	-	-	-
$N_{Ge\text{-}Ge}$	5	12	5	9
$N_{Se\text{-}Se}$	71	69	72	66

Examination of the total neutron structure factors (Figure 5), shows once again that they are very similar whatever the short range chemical disorder introduced by the different models, and also in good agreement with experimental data,[4] as demonstrated in our previous theoretical investigation on ***H*** model.[29] All our graphs exhibit the so-called *first sharp diffraction peak* (FSDP) that is measured experimentally at 1.13 $Å^{-1}$,[4,31] and is associated to intermediate range order, *i.e.* to the second to fourth nearest neighbors. In summary, the usual statistical data ($g_{X\text{-}Y}(r)$, $S_T(\boldsymbol{k})$, …) deduced from the simulations cells give results that are consistent to a point that these quantities can not be considered as the most pertinent ones to discriminate between various glass models.

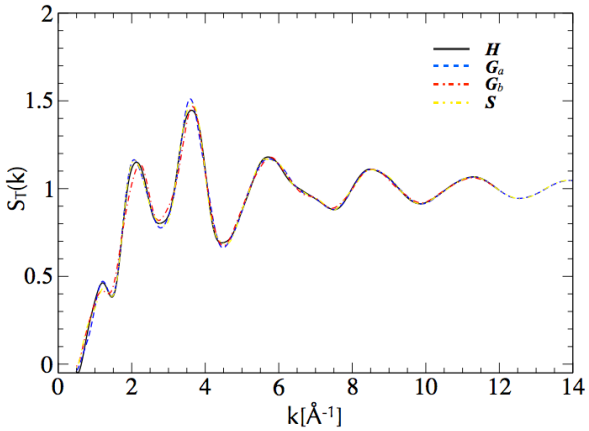

Fig. 5 Total neutron structure factors calculated for the three different glass models : ***H*** (black), G_a (red), G_b (blue) and ***S*** (yellow).

Concerning the relative stability of our various simulated glasses, the energy comparison of several optimized configurations taken from the 300K plateaus shows that the difference between the ***H*** and ***G/S*** models is always below 0.045 eV per atom on average, corresponding therefore to a total energy difference of less than 10 eV between cells and moreover without any particular preference towards one of the models. Consequently this criterion is also not a pertinent one.

Turning to the results of ^{77}Se NMR calculations is however a different story, as it is well known that NMR is much more sensitive to the local organization of the material under investigation. Figure 6 contains the simulated spectra of our heterogeneous models.

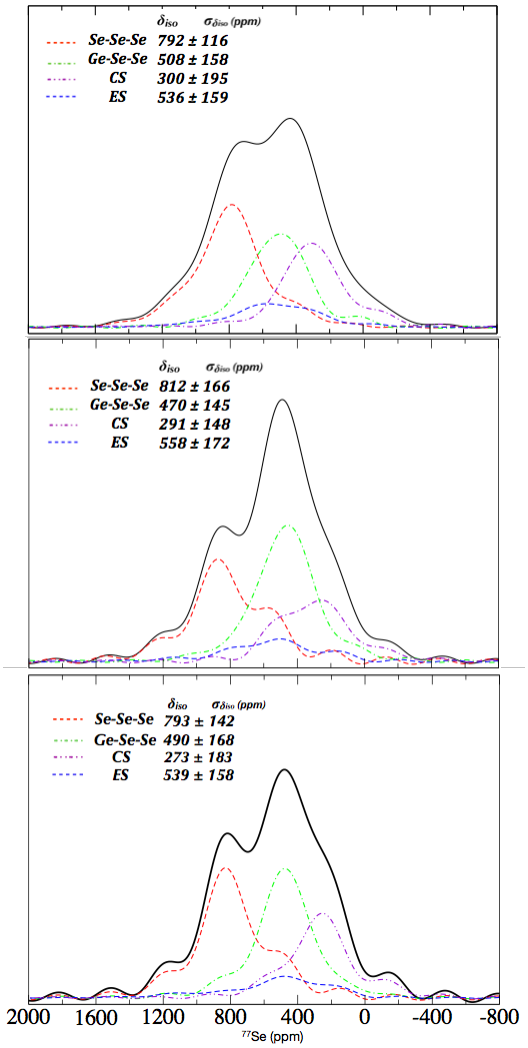

Fig. 6 Simulated ^{77}Se NMR spectra (MAS 23 kHz) obtained for optimized configurations taken from the 300 K plateaus of the ***S*** (top), G_b (middle) and G_a (bottom) models. Contributions of different environments are given, together with the mean ∂_{iso} and standard deviations values.

It is immediately seen that a clear improvement of the spectrum lineshape is obtained with respect to the ***H*** glass (Figure 3) in the case of the ***G*** model. Indeed, for G_a and G_b, two peaks are now resolved in agreement with available experimental data. Furthermore, with respect to spectra presented in Figure 1, it is striking to note that, our systems have spontaneously evolved to give *in silico* glasses characterized by asymmetric ^{77}Se NMR spectra that moreover exhibit a lower height for the resonance associated to the selenium pieces of chains.

From the two kinds of investigated heterogeneous starting configurations, we observed that the ***S*** one leads to the less satisfactory results (Figure 6). This may be related to the fact that the germanium slab is too thin in that case and disappears unrealistically fast (Figure S1). Anyhow, we were able to obtain with the ***G*** starting configurations theoretical signals that more closely match the experimental ones without constructing room temperature cells hand-tuned to specifically exhibit a low fraction of Ge-**Se**-Se units. Upon a closer inspection to our quenched cells, it is clear that the $GeSe_4$ tetrahedra are not evenly distributed in the cell. A selenium-rich area and another one consisting mostly of $GeSe_4$ tetrahedra can be readily identified (Figure 7).

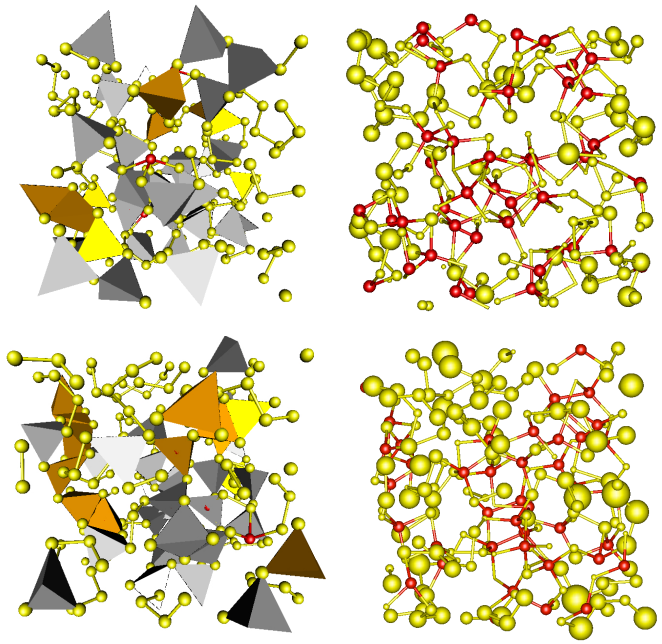

Fig. 7 Visualization, at 300 K, of G_a (bottom) and G_b (top) sample glass cells. Left: GeX_4 (X=Se, Ge) tetrahedra are shown in the structure, right: B&S representation where the size of the Se spheres is proportional to their ∂_{iso} value. Ge – red, Se – yellow, CS tetrahedra – grey, ES polyhedra – orange.

However, they do not fully comply with the *BP* model given that a significant fraction of Ge-**Se**-Se units is found, equal to more than 28% (Table 3). They exhibit a closer agreement with the *RC* one, despite that the deconvoluted percentage of CS selenium atoms is too high by ~15% in the experimental model. Therefore none of the models suggested solely on the basis of experimental deconvolutions fully correspond to our heterogeneous cells. It is worth recalling that both models (*BP* and *RC*) had been introduced in order to account of the typical double-resonance 1D-NMR lineshape, assuming that no Ge-Ge bonds were involved. From the results of the present work, it appears that such models were useful but are probably more suited to give a qualitative picture of the glass structure.

Table 3. Distribution of the various selenium environment fractions (%) in the theoretical models of this work

	G_a	G_b	S
Se-Se-Se	35	31	35
Ge-Se-Ge	30	29	33
CS	22	20	23
ES	8	9	10
Ge-Se-Se	32	36	28
Se$_*$[a]	2	4	3

[a]denotes all Se atoms deviating from the 8-N rule.

Examination of the selenium environments in the ***G*** and ***S*** models, shows that the percentage of Ge-**Se**-Se units is calculated, as anticipated, to be lower with respect to the ***H*** model (Tables 1 and 3). However, contrary to our expectations, this reduction may be rather low (***G$_b$***) and seems to benefit mostly to the Se-**Se**-Se chains. A comparison of the lineshapes with respect to the various X-**Se**-X (X=Se, Ge) fractions shows that these quantities are not sufficient on their own to draw definitive conclusions. Indeed, very nice ^{77}Se NMR signals may be obtained with Ge-**Se**-Se fractions up to ~32% (***G*** models), while the ***S*** model exhibits a lower value but leads to a less pertinent signal.

Generally speaking, it is also interesting to note that structural variations in the MD glass configurations can be detected (even with the same models, see figure 6) due to modifications of the NMR lineshape, thank to the high sensitvity of ^{77}Se solid-state NMR. On the other hand, as shown above, the Radial Distribution Functions (Figure S4) and the total neutron factors (Figure 5) are almost undistinguishable, whatever the starting-points considered in this work, *i.e.* homogeneous or strongly heterogeneous ones.

Conclusions

Quantitative solid-state ^{77}Se NMR experimental spectra have been obtained on isotopically enriched as well as natural abundance samples. Consistent modifications of the experimental spectrum have been observed in the two cases, with respect to earlier ^{77}Se NMR investigations, provided that long enough recovery delays are employed. This work demonstrates that ^{77}Se spin-lattice relaxation times in $GeSe_4$ are much longer than previously assumed. This observation makes possible the acquisition of a new ^{77}Se referenced spectrum for $GeSe_4$ glasses.

Concerning the theoretical side of this work, we have shown that MD simulations beginning from randomly distributed Ge and Se atoms configurations, *i.e.* bypassing the mixing phase, lead to excessively homogeneous structural models which do not account for the experimental spectra. Incorporating the mixing phase and therefore matching more closely the experimental synthetic process, allows the resolution of the observed NMR spectrum discrepancy and to achieve a good agreement with the new ^{77}Se NMR experiments. We note that $GeSe_4$ structures successfully matching the NMR spectrum show heterogeneity, in particular as regards the distribution of the germanium tetraedra in the network.

As a summary, significant progresses have been made simultaneously on the experimental and theoretical sides in the structural characterization of the $GeSe_4$ glass, which enables a deep refinement as compared to the previous models. More generally speaking, these results give new prospects, both experimentally and on the calculation aspects, for the elucidation of the structure and properties of chalcogenide glasses.

Acknowledgements

This work was granted access to the HPC resources of IDRIS under the allocation **2013-086045** made by GENCI (Grand Equipement National de Calcul Intensif). The TGIR-RMN-THC is gratefully acknowlegded for providing access to their spectrometers.

Notes and references

[a] Institut des Sciences Chimiques de Rennes - UMR 6226 - ENSCR, 11 allée de Beaulieu, CS50837, 35708 Rennes Cedex 7, France
[b] Institut des Sciences Chimiques de Rennes - UMR 6226, 263 avenue du Général Leclerc, 35042 Rennes Cedex, France
[c] CEMHTI, CNRS UPR 3079, 1D Avenue de la Recherche Scientifique, 45071 Orléans cedex 2, France
[d] Department of Physics and Astronomy, University College London, Gower Street, London WC1E 6BT, UK

Electronic Supplementary Information (ESI) available: Evolution of the Ge-Ge bond percentage in the liquid state, Influence on the spectrum of the optimization process, Impact of the energy cut-off on the calculated chemical shieldings and simulated spectrum, Theoretical Radial distribution functions at 300 K for the three models, Influence on the lineshape of taking into account dispersion corrections, description of the starting configurations setup. See DOI: 10.1039/b000000x/

1 A. Zakery, S. Elliott, *J. Non-Cryst. Solids* **2003**, *330*, 1–12.
2 X. Zhang, B. Bureau, P. Lucas, C. Boussard-Pledel, J. Lucas, *Chem. Eur. J.* **2008**, *14*, 432–442.
3 A. Pereira Gonçalves, E. Branco Lopes, O. Rouleau, C. Godart, *J. Mater. Chem.* **2010**, *20*, 1516–1521.
4 L. Petri, P. S. Salmon, *Phys. Chem. Glasses C* **2002**, *43*, 185–190.
5 V. Petkov, D. Le Messurier, *J. Phys. - Condens. Mat.* **2010**, *22*, 115402.
6 T. G. Edwards, S. Sen, *J. Phys. Chem. B* **2011**, *115*, 4307–4314.
7 B. Bureau, J. Troles, M. Le Floch, P. Guénot, F. Smektala, J. Lucas, *J. Non-Cryst. Solids* **2003**, *319*, 145–153.
8 M. F. Thorpe, *J. Non-Cryst. Solids* **1983**, *57*, 355–370.
9 P. Lucas, E. A. King, O. Gulbiten, J. L. Yarger, E. Soignard, B. Bureau, *Phys. Rev. B* **2009**, *80*, 214114.
10 E. L. Gjersing, S. Sen, B. G. Aitken, *J. Phys. Chem. C* **2010**, *114*, 8601–8608.
11 T. G. Edwards, S. Sen, E. L. Gjersing, *J. Non-Cryst. Solids* **2012**, *358*, 609–614.
12 D. C. Kaseman, I. Hung, Z. Gan, S. Sen, *J. Phys. Chem. B* **2013**, *117*, 949–954.
13 M. Kibalchenko, J. R. Yates, C. Massobrio, A. Pasquarello, *J. Phys. Chem. C* **2011**, *115*, 7755–7759.

14 a) H. Y. Carr, E. M. Purcell, *Phys. Rev.* **1954**, *94*, 630. b) S. Meiboom D. Gill, *Rev. Sci. Instrum.* **1958**, *29*, 688.
15 R. Car, M. Parrinello, *Phys. Rev. Lett.* **1985**, *55*, 2471–2474.
16 W. Andreoni, A. Curioni, *Parallel Comput.* **2000**, *26*, 819–842.
17 D. Marx, J. Hutter, Ab-initio Molecular Dynamics: Theory and Implementation. In *Modern Methods and Algorithms of Quantum Chemistry*; Grotendorst, J., Ed.; Forschungszentrum Jülich, **2000**; 301–449.
18 J. P. Perdew, K. Burke, M. Ernzerhof, M. *Phys. Rev. Lett.* **1996**, *77*, 3865–3868.
19 N. Troullier, J. L. Martins, *Phys. Rev. B* **1991**, *43*, 8861–8869.
20 N. Troullier, J. L. Martins, *Phys. Rev. B* **1991**, *43*, 1993–2006.
21 S. Nosé, *Mol. Phys.* **1984**, *52*, 255–268.
22 W. Hoover, *Phys. Rev. A* **1985**, *31*, 1695–1697.
23 C. Pickard, F. Mauri, *Phys. Rev. B* **2001**, *63*, 1–13.
24 S. J. Clark, M.D. Segall, C. J. Pickard, P. J. Hasnip, M. I. J. Probert, K. Refson, M. C. Payne, *Z. Kristallogr.* **2005**, *220*, 567–570.
25 U. Haeberlen, *High Resolution NMR in Solids: Selecxtive Averaging*; Academic Press, New York:, **1976**.
26 M. Kibalchenko, J. Yates, C. Massobrio, A. Pasquarello, *Phys. Rev. B* **2010**, *82*, 2–5. 0202002
27 M. Bak, J. T. Rasmussen, N. C. Nielsen, *J. Magn. Reson.* **2000**, *147*, 296–330.
28 C. Bonhomme, C. Gervais, F. Babonneau, C. Coelho, F. Pourpoint, T. Azas, S. E. Ashbrook, J. M. Griffin, J. R. Yates, F. Mauri, C. J. Pickard *Chem. Rev.* **2012**, 112, 5733−5779 and references therein.
29 K. Sykina, E. Furet, B. Bureau, S. Le Roux, C. Massobrio, *Chem. Phys. Lett.* **2012**, 30–34.
30 C. Massobrio, M. Celino, P. S. Salmon, R. Martin, M. Micoulaut, A. Pasquarello, A. *Phys. Rev. B* **2009**, *79*, 174201.
31 L. B. Skinner, C. J. Benmore, S. Antao, E. Soignard, S. A. Amin, E. Bychkov, E. Rissi, J. B. Parise, J. L. Yarger, *J. Phys. Chem. C* **2012**, *116*, 2212–2217.